electronics

MDPI

Article

Coverage Enhancement of Light-Emitting Diode Array in Underwater Internet of Things over Optical Channels

Anliang Liu [1], Huiping Yao, Haobo Zhao, Yingming Yuan and Yujia Wang *

School of Information Science and Technology, Dalian Maritime University, Dalian 116026, China; alliu@dlmu.edu.cn (A.L.); xinping@dlmu.edu.cn (H.Y.); zhb2022@dlmu.edu.cn (H.Z.); yym0199@dlmu.edu.cn (Y.Y.)

* Correspondence: yujiawang@dlmu.edu.cn

Abstract: The construction of the underwater Internet of Things (UIoT) is crucial to marine resource development, environmental observation, and tactical surveillance. The underwater optical wireless communication (UOWC) system with its large bandwidth and wide coverage facilitates the high-capacity information interconnection within the UIoT networks over short and medium ranges. To enhance the coverage characteristics of the UOWC system, an optimized lemniscate-compensated layout of light-emitting diode (LED) array is proposed in this paper, which can ameliorate the received optical power and reliability at the receiving terminal. Compared with traditional circular and rectangular layouts, the received optical power and bit error rate (BER) performance of the proposed system are analyzed based on the Monte Carlo simulation method. The analysis results show that the proposed LED array achieves a smaller peak power deviation and mean square error of the received optical power under three typical seawater environments. Furthermore, the proposed LED-array scheme supports a better BER performance of the UOWC system. For example, in turbid seawater with a transmission depth of 9.5 m, the BER of the proposed LED array layout is 1×10^{-7}, which is better than the BER of 3.5×10^{-6} and 1×10^{-4} under the other two traditional light source layouts.

Keywords: underwater optical wireless communication; underwater Internet of Things; Monte Carlo model; LED array

Citation: Liu, A.; Yao, H.; Zhao, H.; Yuan, Y.; Wang, Y. Coverage Enhancement of Light-Emitting Diode Array in Underwater Internet of Things over Optical Channels. *Electronics* **2023**, *12*, 4736. https://doi.org/10.3390/electronics12234736

Academic Editors: Shibo He, Huan Zhou, Victor C. M. Leung, Fangyuan Xing and Lei Yang

Received: 7 November 2023
Revised: 18 November 2023
Accepted: 20 November 2023
Published: 22 November 2023

1. Introduction

Compared with underwater radio frequency (RF) communication and underwater acoustic communication, the underwater optical wireless communication (UOWC) system has many advantages including high bandwidth, low time latency, and great security [1]. UOWC is widely applied in marine resources exploration, environment monitoring, and marine defense [2,3]. Especially for underwater Internet of Things (UIoT) scenarios, a strong robust communication system with high flexibility is necessary to realize information interaction between mobile nodes such as autonomous underwater vehicle (AUV) swarms, or between AUV and underwater fixed sensor networks. Therefore, the UOWC system based on the light-emitting diode (LED) light source has attracted more attention due to its advantages of large divergence angle, low system costs, and temperature insensitivity, which makes it more suitable for the high-speed interconnection of UIoT devices at short and medium ranges. In addition, LED light sources can be effectively compatible with underwater lighting equipment, and the progress of LED technology in recent years has enabled high-dynamic UOWC systems with small size and low power consumption [4].

Complex underwater channel environments, including absorption, scattering and turbulence effects, are the main constraints on the communication performance of UWOC systems [5–7]. Underwater channel modeling is the primary requirement for analyzing the transmission characteristics of optical signals under different seawater conditions.

Commonly used methods of underwater channel modeling are based on the Beer–Lambert law and radiative transfer equation (RTE) [8]. The Beer–Lambert law is generally used to evaluate the transmission loss of the optical signal power without considering the scattering effect. The RTE method describes the energy conservation for light propagating over an absorbing and scattering medium [9]. However, RTE is expressed by an integro-differential equation, which makes it complicated to achieve analytical solutions. The Monte Carlo (MC) simulation evaluates the transmission characteristics of the system by tracking large numbers of photons, and has become the most widely used RTE numerical solution method in recent years due to its high flexibility and accuracy [10]. Geldard et al. proposed a method to model turbulence as a scattering phenomenon, and used double gamma function to simulate the frequency response of three different turbulence values in harbor seawater [11]. Combining the stochastic model with the lognormal turbulence model, the BER performance of the multiple-input single-output (MISO) UOWC systems was evaluated under weak turbulence, absorption, and scattering conditions [12]. A comprehensive channel model with absorption, scattering, and weak turbulence effects was considered, and the optimal power allocation policies were obtained to achieve smaller bit error rates (BERs) for both MISO and multiple-input multiple-output (MIMO) systems [13].

Most of the above studies are focused on point-to-point underwater link structures by using the MC simulation method. For underwater highly dynamic and complex channel scenarios, it is difficult to maintain the relative stability of the transceiver to ensure link alignment [14]. At the receiving terminal, a lens array structure was proposed to achieve effective convergence of received optical signals at different incident angles, which can improve the dynamic response range of the receiver [15]. On the other hand, common optimization methods focus on using LED arrays at the transmitting terminal to enhance the signal coverage, which can also alleviate the alignment requirements of UOWC systems over short and medium ranges. Therefore, for the LED array-based UOWC system, it is more important to improve the system robustness under complex dynamic seawater environments through the optimization of the LED array, which in turn reduces the alignment difficulty of the UOWC system. Ding et al. proposed an evolutionary algorithm to optimize the optical intensity of LED transmitters for reducing the signal power fluctuation [16]. An improved genetic simulated annealing algorithm was proposed to reduce the power fluctuation and improve the coverage uniformity of the indoor visible light communication (VLC) system [17]. Random geometries were considered to improve the power allocation for uniform illumination in the VLC system [18]. In [19], an improved artificial fish swarm algorithm was proposed for adjusting the horizontal layout of the LED array. To improve the coverage characteristics, the half-power angle and horizontal layout were optimized by an improved BAT algorithm in [20], which can effectively reduce the illumination fluctuation with different LED arrays.

The above algorithms are mostly used in indoor VLC systems without considering the complexity of underwater channels and the underwater spatial coverage characteristics of the LED array sources, which is of great significance for realizing a wide optical signal coverage. The optimization of the LED array scheme is crucial to ameliorating the received optical power and reliability in the UOWC system. In our previous work [21], an optimized LED array was proposed to achieve a uniform coverage characteristics. However, the system had many optimization parameters, which is not conducive to implementation in a limited underwater space. Moreover, the simulation only included the analysis of the received optical power uniformity and lacked analysis on the reliability of the UOWC system.

In this paper, considering the complexity of underwater system implementation, a lemniscate-compensated layout is proposed to enhance the coverage efficiency of the underwater LED array and communication performance of UOWC system in complex environments, which is essential to achieve high-speed and dynamic reliable communication over short and medium ranges in the UIoT network. Based on the MC simulation method, taking a 16-LED array as an example, the received optical power distribution and

the BER performance of the proposed LED array-based UOWC system are analyzed in detail by comparing with the traditional ellipse-compensated layout and ring-compensated layout under different seawater types at different transmission depths. The simulation results verify that the proposed system has better performance in terms of signal coverage characteristics and communication performance.

The remainder of the paper is organized as follows. Section 2 presents the system model, including absorption and scattering effects, the MC simulation method, and the BER analysis. The schemes of the LED array layouts and simulation setup are first given in Section 3. Then, the results, including the fluctuation and uniformity of the received optical power, and BER performance are presented and discussed. Finally, the conclusions and future work directions are given in Section 4.

2. System Model

2.1. Absorption and Scattering

The underwater propagation of light is mainly affected by the absorption and scattering effect, which decreases light power greatly and influences the transmission direction of light. Then, the total attenuation coefficient $c(\lambda)$ of the light beam through the seawater medium can be expressed as [22]

$$c(\lambda) = a(\lambda) + b(\lambda) \tag{1}$$

where $a(\lambda)$ represents the absorption coefficient and $b(\lambda)$ represents the scattering coefficient. They are related to the wavelength with the unit of m^{-1}. The widely used absorption and scattering coefficients for three typical seawater environments, including clean seawater, coastal seawater, and harbor seawater, were measured by Petzold in [9]. All coefficient parameters are shown in Table 1. As the turbidity of seawater increases, the total attenuation coefficient becomes larger, which means that the transmission distance and quality of the light signal are severely restricted in complex seawater environments.

Table 1. Attenuation coefficient of different seawater environments.

Typical Seawater	a (m^{-1})	b (m^{-1})	c (m^{-1})	Albedo
clean seawater	0.114	0.037	0.151	0.25
coastal seawater	0.179	0.219	0.398	0.55
harbor seawater	0.366	1.824	2.190	0.83

2.2. MC Simulation Method

We use the MC simulation method to simulate the propagation trajectory of photons through complex seawater environments, and evaluate the transmission characteristics by counting the state information of photons at the receiving terminal. The flow chart of the MC simulation method is shown in Figure 1.

The LED light source used in our UOWC system model can be defined by the generalized Lambertian light sources. The distribution of radiant intensity $\Psi(\theta_0)$ can be expressed as [23]

$$\psi(\theta_0) = \frac{1+m}{2\pi}\cos^m(\theta_0) \tag{2}$$

$$m = -\ln 2 / \ln[\cos(\theta_{1/2}/2)] \tag{3}$$

where θ_0 is the zenith angle, m is the radiation mode coefficient of the light source, and $\theta_{1/2}$ is the semi-angle at half-power of the light source.

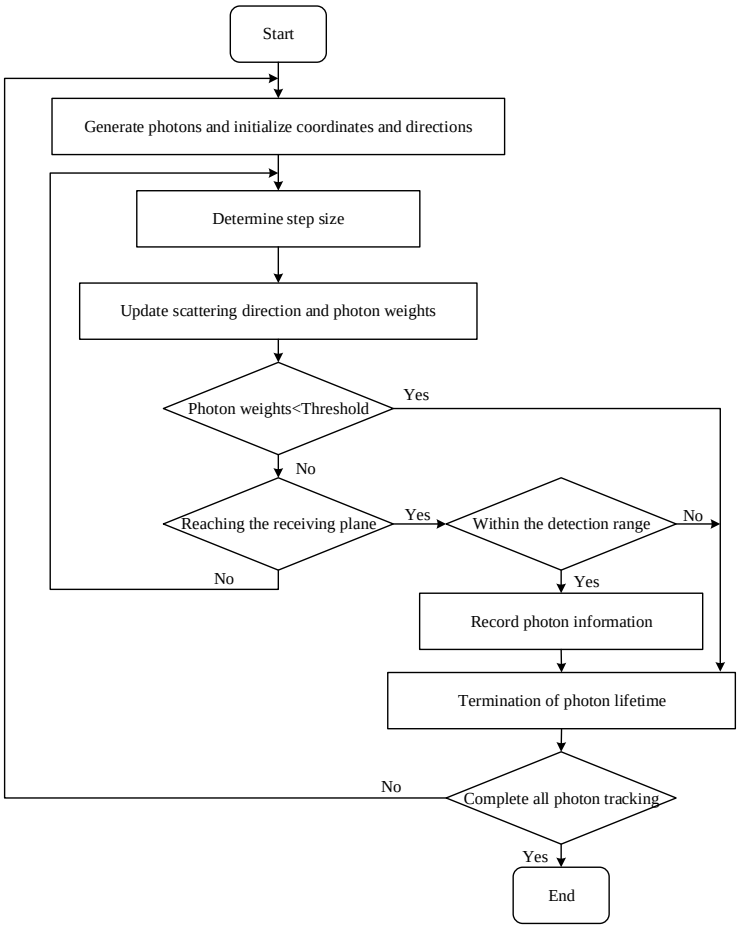

Figure 1. MC simulation method flow chart.

The step size s of a photon is the distance that the photon moves in the seawater before scattering and absorption. It can be expressed as [24]

$$s = -\frac{\ln(\eta)}{c} \tag{4}$$

where η is a uniform random number between 0 and 1.

The emitted photons are affected by the seawater channel during underwater transmission, where the absorption effect reduces the weight of the photon, and the scattering effect changes the propagation direction. The weight W_{pos} of the photon after the scattering can be expressed as

$$W_{pos} = W_{pre} \cdot r \tag{5}$$

where W_{pre} is the weight before photon scattering. The albedo r describes the weight loss of photons after the scattering and is given by $r = b/c$.

After the photon weight is determined, we need to further obtain the scattering angle of the photon to evaluate its movement direction. And the probability distribution of photon propagation directions usually follows the volume scattering function (VSF). It is difficult to measure the VSF, and the most widely cited scattering measurement is the Petzold average phase function. Moreover, several types of analytical phase functions, such as the Henyey–Greenstein (HG), two-term Henyey–Greenstein (TTHG), and Fournier–Forand (FF), have been proposed. The variation of different scattering phase functions is shown in Figure 2.

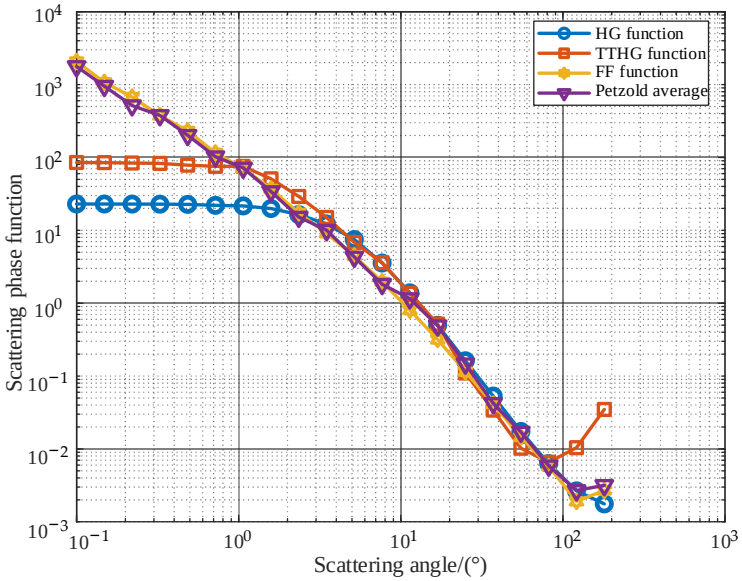

Figure 2. Comparison of scattering phase functions.

The HG phase function is a convenient and simple way to achieve an easy computation of the RTE. However, the phase function has a large difference compared with the Petzold average when the scattering angle approaches 0° and 180°. The TTHG function also underestimates Petzold's measurement of scattering angle < 1°. The FF function is used to fit the measurement results. The root mean square value of the fitting results and the experimental results is 15.3, which is closer to the real seawater scattering phase function. Therefore, the FF function can be used as the seawater scattering phase function to generate the zenith angle and azimuth angle of photons. The zenith angle using the FF scattering phase function $\beta_{FF}(\theta)$ can be obtained by [9]

$$2\pi \int_0^{\theta} \beta_{FF}(\theta') \sin\theta' d\theta' = \varepsilon \tag{6}$$

$$\beta_{FF}(\theta) = \beta_0(\theta) + \beta_0(\pi)(3\cos^2\theta - 1)/4 \tag{7}$$

$$\beta_0(\theta) = \frac{1}{4\pi} \frac{1}{(1-\delta)^2 \delta^v} \times \left\{ [v(1-\delta) - (1-\delta^v)] + \frac{4}{u^2}[\delta(1-\delta^v) - v(1-\delta) \right\} \tag{8}$$

$$\delta = \frac{u^2}{3(n-1)^2} \tag{9}$$

$$v = \frac{(3-u)}{2} \tag{10}$$

$$u = 2\sin(\theta/2) \tag{11}$$

where u is the exponential term and n is the refractive index.

The azimuth φ after scattering follows a uniform distribution between 0 and 2π. It can be given by

$$\varphi = 2\pi\varepsilon \tag{12}$$

where ε is a uniform random number between 0 and 1.

2.3. BER Performance Analysis

The on-off keying (OOK) modulation scheme is one of the most popular modulation formats in underwater wireless optical communication systems because of its simple

implementation and low cost. Therefore, we employ the OOK modulation to further evaluate the BER performance of the proposed UOWC system [25]. It is assumed that the original data sequence x is $[x_1, x_2,..., x_i,..., x_N]$, $x_i = 0$ or 1. The transmission power $P_s(t)$ can be expressed as [26]

$$P_s(t) = \sum_{n=1}^{N} x_n Z(t - nT) \tag{13}$$

where T is the time interval of the data, and $Z(t)$ is the gate function with the width of T. The receiving power $P_r(t)$ is the convolution of the transmission power and the impulse response of the UOWC channel, which can be expressed as

$$P_r(t) = \sum_{n=1}^{N} x_n Z(t - nT) * h(t - nT) \tag{14}$$

The decision of the receiving sequence $y = [y_1, y_2, \ldots, y_i, \ldots, y_N]$ can be obtained by comparing the sample value y' with the threshold value T_{thr}, which can be expressed as [27]

$$y^{'} = \sum_{m=1}^{M} y_m^{'} / M \tag{15}$$

$$T_{thr} = \frac{\sigma_0 \mu_1 + \sigma_1 \mu_0}{\sigma_0 + \sigma_1} \tag{16}$$

where M is the number of samples. u_0 and u_1 are the mean values of the received signals "0" and "1", and σ_0 and σ_1 are the variances of the received signal "0" and "1".

The judgment rules are given by

$$y_i = \begin{cases} 0 & y^{'} < T_{thr} \\ 1 & y^{'} > T_{thr} \end{cases} \tag{17}$$

Then, the BER of the UOWC system with OOK modulation P_E is given by

$$P_E = Q(A_n) \tag{18}$$

where

$$A_n = \frac{\mu_0 + \mu_1}{\sigma_0 + \sigma_1} \tag{19}$$

$$Q(x) = \frac{1}{\sqrt{2\pi}} \int_x^{\infty} e^{-t^2/2} dt \tag{20}$$

3. Simulation Analysis and Results

3.1. Layout Design of LED Array

The underwater channel model is established using the MC simulation method. A lemniscate-compensated layout of the LED array is proposed, and its performance is compared with two other traditional layouts, an ellipse-compensated layout and a ring-compensated layout. Taking 16-LED light sources as an example, three different layout schemes are shown in Figure 3. For the ellipse-compensated layout as shown in Figure 3a, twelve LED light sources are evenly arranged as an ellipse in the central area, which is simple to implement. For the ring-compensated layout as shown in Figure 3b, eight LED light sources and four LED light sources are distributed in an outer ring and an inner ring, respectively, and the emission power is concentrated in the central area. For the lemniscate-compensated layout, twelve LED light sources are arranged as shown in Figure 3c, with two LED light sources set at the center so that the number of LEDs is consistent with the other two layouts. Additionally, to improve the uniformity of optical signal coverage at the transmitting end, four compensation light sources are arranged at the corners of each LED layout, respectively.

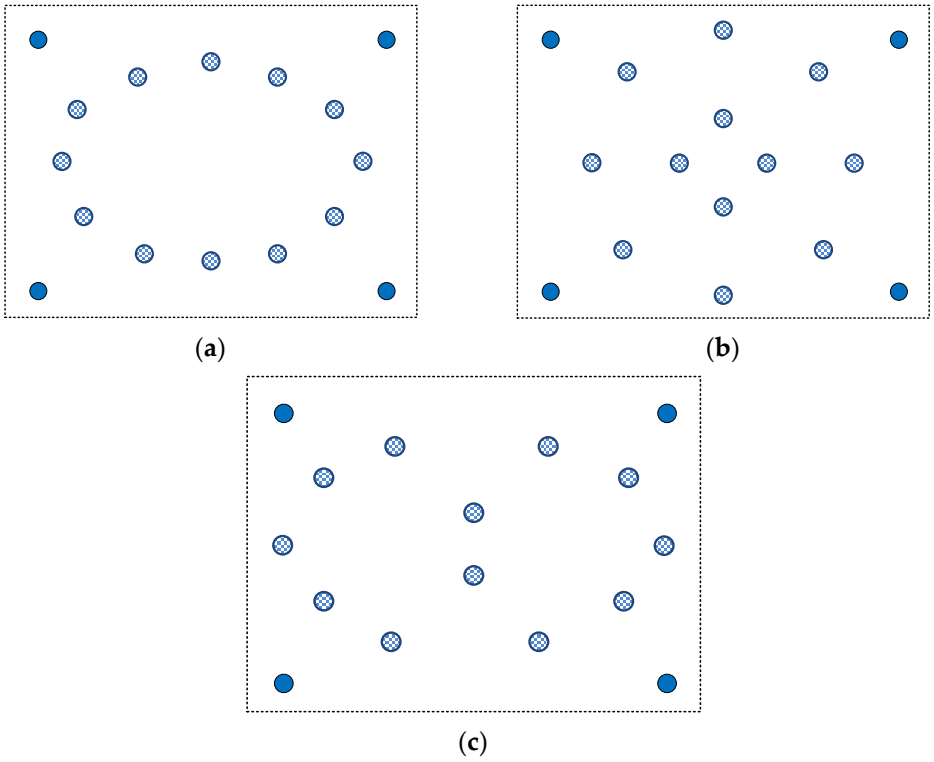

Figure 3. (**a**) Ellipse-compensated layout; (**b**) ring-compensated layout; (**c**) lemniscate-compensated layout.

3.2. Simulation Setup

Taking the ellipse-compensated layout as an example, the system model is shown in Figure 4. Assuming that the size of the spatial area to be covered is 10 m × 10 m × d. The LED light sources are located on the X-0-Y plane, and the initial position of the LED light source is (X_i, Y_i, 0). The receiving plane is parallel to the transmitting plane with a depth of d m.

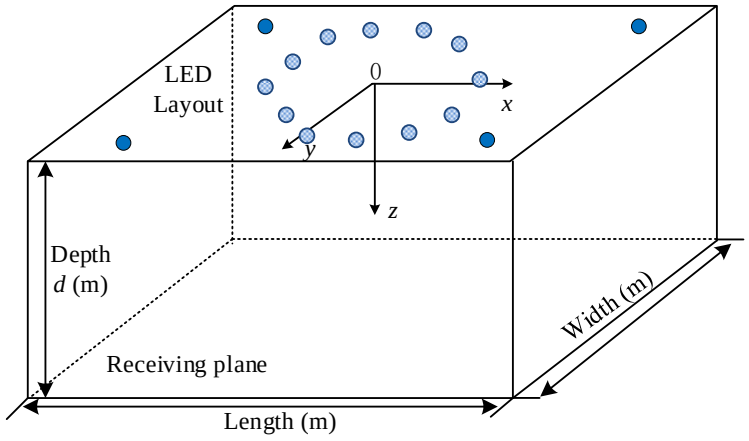

Figure 4. Schematic diagram of ellipse-compensated layout.

The number of LED light sources used in the three light source layouts is 16. The positions of LED light source in the ellipse-compensated layout are (2.2, 0, 0), (−2.2, 0, 0), (1.83, 1.06, 0), (1.83, −1.06, 0), (−1.83, 1.06, 0), (−1.83, −1.06, 0), (0, 1.9, 0), (0, −1.9, 0), (0.98, 1.70, 0), (0.98, −1.70, 0), (−0.98, 1.70, 0), and (−0.98, −1.70, 0). The positions of LED light sources in the ring-compensated layout are (0, 1, 0), (0, −1, 0), (1, 0, 0), (−1, 0, 0), (0, 2, 0), (0, −2, 0), (2, 0, 0), (−2, 0, 0), (1.41, 1.41, 0), (1.41, −1.41, 0), (−1.41, 1.41, 0), and (−1.41, −1.41, 0), respectively. The LED positions in the lemniscate-compensated layout are (2.2, 0, 0),

(−2.2, 0, 0), (1.87, 1.1, 0), (1.87, −1.1, 0), (−1.87, 1.1, 0), (−1.87, −1.1, 0), (1.2, 1.9, 0), (1.2, −1.9, 0), (−1.2, 1.9, 0), (−1.2, −1.9, 0), (0, −1.1, 0), and (0, 1.1, 0), respectively. The positions of the four compensated light sources are (2.2, 1.9, 0), (2.2, −1.9, 0), (−2.2, 1.9, 0), and (−2.2, −1.9, 0). The detail simulation parameters used in the UOWC system model are shown in Table 2.

Table 2. System simulation parameters [28].

Parameters	Value
quantity of LED array	16
divergence angle	20°
pattern length	$2^{20} - 1$
receiver field of view	180°
size of receiving plane	10 m × 10 m
data rate	0.1 Gbps

3.3. Results and Discussion

3.3.1. Received Optical Power Distribution

The underwater spatial irradiance characteristics of the different LED light source layouts are simulated and analyzed using MATLAB 9.6 software. First, we compare the performance of the received optical power after it is transmitted over different underwater depths with three LED array layouts. Taking the coastal seawater environment as an example, the power distribution performance for the receiving planes is measured with the transmission depths of 5 m, 7 m, and 9 m, respectively, as shown in Figure 5.

It can be seen from Figure 5 that the maximum received optical power of the three different LED array layouts, affected by the underwater channel environments, decreases from 27.42 dBm to 18.60 dBm, 28.93 dBm to 19.54 dBm, and 27.96 dBm to 18.77 dBm, respectively, as the transmission depth increases. The maximum received optical power of the ring-compensated layout is the largest, since the LED light sources are relatively concentrated in the central area of the transmitter. At the same time, the maximum received optical power of this layout also decreases the fastest after underwater transmission. However, considering the complex characteristics of the underwater environment, to further simplify the alignment operation of the transceivers and improve the dynamic response capability of the UOWC system, a smaller fluctuation of the received optical power is more important to ensure the reliability of the communication link. Therefore, we define the peak power deviation (PPD) index to evaluate the fluctuation of the received optical signals, and the PPD is given by the ratio of the maximum received optical power to the minimum received optical power. The PPD results of the three LED layouts at different coastal seawater depths are shown in Table 3. It can be seen that the PPD of the lemniscate-compensated layout is 0.79, which is 0.02 less than the ellipse-compensated layout and 0.1 less than the ring-compensated layout at a depth of 5 m in coastal seawater. At a depth of 7 m in coastal seawater, the PPD of the lemniscate-compensated layout is 0.66, which is 0.02 less than the ellipse-compensated layout and 0.09 less than the ring-compensated layout. At a depth of 9 m in coastal seawater, the PPD of the lemniscate-compensated layout is the lowest compared with the ellipse-compensated layout and the ring-compensated layout. The receiving power fluctuation of the lemniscate-compensated layout is lower than that of the other two layouts when propagating 5 m, 7 m, and 9 m in coastal seawater, which means that the uniformity of the received optical power is improved in the proposed UOWC system.

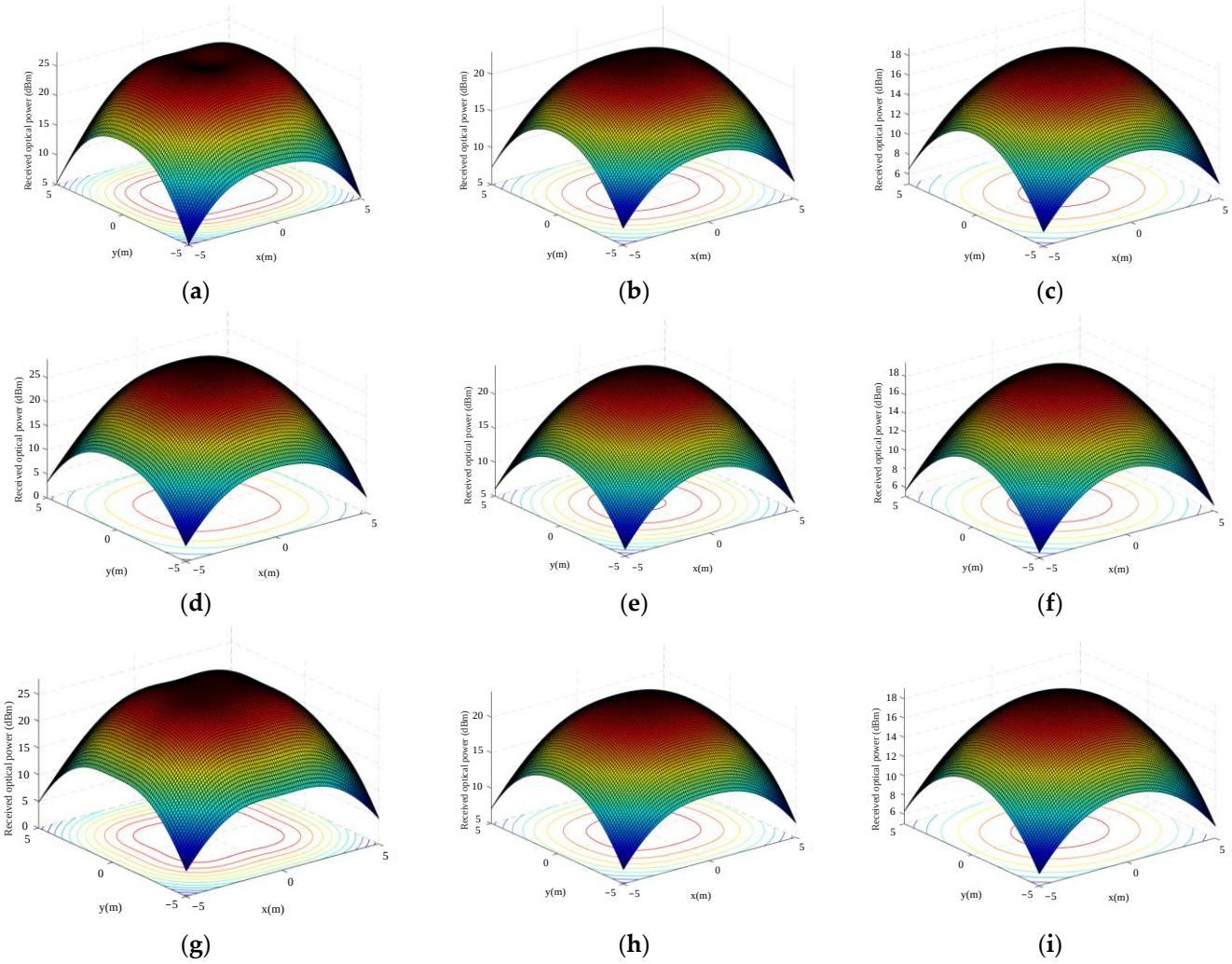

Figure 5. Received optical power distribution for three layouts at different depths in coastal seawater. Ellipse-compensated layout at (**a**) 5 m; (**b**) 7 m; and (**c**) 9 m; ring-compensated layout at (**d**) 5 m; (**e**) 7 m; and (**g**) 9 m; and lemniscate-compensated layout at (**g**) 5 m; (**h**) 7 m; and (**i**) 9 m.

Table 3. Analysis of received optical power.

Transmission Depth (m)	LED Layout	Maximum Received Power (dBm)	Minimum Received Power (dBm)	PPD
5 m	ellipse-compensated layout	27.42	5.20	0.81
	ring-compensated layout	28.93	3.27	0.89
	lemniscate-compensated layout	27.96	5.76	0.79
7 m	ellipse-compensated layout	23.08	7.31	0.68
	ring-compensated layout	24.30	6.00	0.75
	lemniscate-compensated layout	23.07	7.94	0.66
9 m	ellipse-compensated layout	18.60	6.01	0.68
	ring-compensated layout	19.54	5.60	0.71
	lemniscate-compensated layout	18.77	6.46	0.65

3.3.2. Mean Square Error

The received optical power fluctuation and uniformity of the three LED layouts under three typical seawater environments at different transmission depths are further analyzed by calculating the root mean square error (RMSE) of the received optical power. Dividing the receiving plane into a 100 × 100 micro area, the RMSE of the received optical power can be given by

$$\mathrm{RMSE} = \sqrt{\sum_{i=1}^{N} (P_i - P_{mean})^2 / N} \tag{21}$$

where P_i is the receiving power of each micro area on the receiving plane, P_{mean} is the average receiving power, and N is the number of micro area sources on the receiving plane.

In Figure 6, the RMSE of the three LED layouts at different transmission depths is measured under three typical seawater environments. In clean seawater, the overall fluctuation of the RMSE of the lemniscate-compensated layout is much better than that of the traditional ellipse-compensated and ring-compensated layouts. It can be seen from Figure 6a that, at a depth of 3 m, the RMSE of the lemniscate-compensated layout is 4.9, which is 0.2 less than the ellipse-compensated layout and 0.9 less than the ring-compensated layout. In coastal seawater, the overall RMSE of the lemniscate-compensated layout is lower than the traditional ellipse-compensated layout and ring-compensated layout. At a depth of 3 m in coastal seawater, the RMSE of the lemniscate-compensated layout is 4.6, which is 0.6 less than the ellipse-compensated layout and 1.2 less than the ring-compensated layout. In harbor seawater, the RMSE of the proposed lemniscate-compensated layout is 7 at a depth of 3 m, which is also lower than that of the traditional layouts. It can be seen that the lemniscate-compensated layout has relatively small received power fluctuation and can support more reliable communication under all three seawater types. Particularly, the RMSE of the received optical power increased at a transmission depth greater than 3 m, which indicates that the distribution uniformity of the received optical power becomes worse due to the larger attenuation coefficient of harbor seawater. Figure 7 shows the distribution of the received optical power at a transmission depth of 5 m in harbor seawater. It can be seen that the received optical power reduces to the range of -25 dBm to -50 dBm, which makes it difficult to achieve reliable communication for the UOWC system. Therefore, while analyzing the uniformity of the optical signal, the received optical power and system BER performance should be further analyzed based on the received optical power information obtained under different layouts to determine the reliable communication range of the proposed UOWC system.

3.3.3. BER Performance

By analyzing the BER results, we can evaluate the performance of the UOWC system based on different LED layouts. The BER curves of the three layouts in clean seawater, coastal seawater, and harbor seawater at different depths are shown in Figure 8. It can be seen that the BER of the lemniscate-compensated layout is lower than that of the other two traditional LED layouts. In clean seawater, the BER for the lemniscate-compensated layout at a 13 m depth is 1×10^{-8}. The ellipse-compensated and ring-compensated layouts' BERs are 1.5×10^{-7} and 6.5×10^{-7}, respectively. The transmission distance with the lemniscate-compensated LED layout is longer than the traditional layouts under the same BER. In coastal seawater, the BER of the three compensated layouts varies significantly with distance transmission. The BER of the lemniscate-compensated layout is 1×10^{-7}, which is better than the BER of 3.5×10^{-6} and 1×10^{-4} under the other two traditional light source layouts at a depth of 9.5 m. In the harbor seawater, the BER of the lemniscate-compensated layout, ellipse-compensated layout, and ring-compensated layout is 2.5×10^{-5}, 6×10^{-5}, and 1.8×10^{-4} at a depth of 2 m. Compared with the traditional layouts, the BER performance of the proposed lemniscate-compensated layout is better under different seawater types at the same transmission depth.

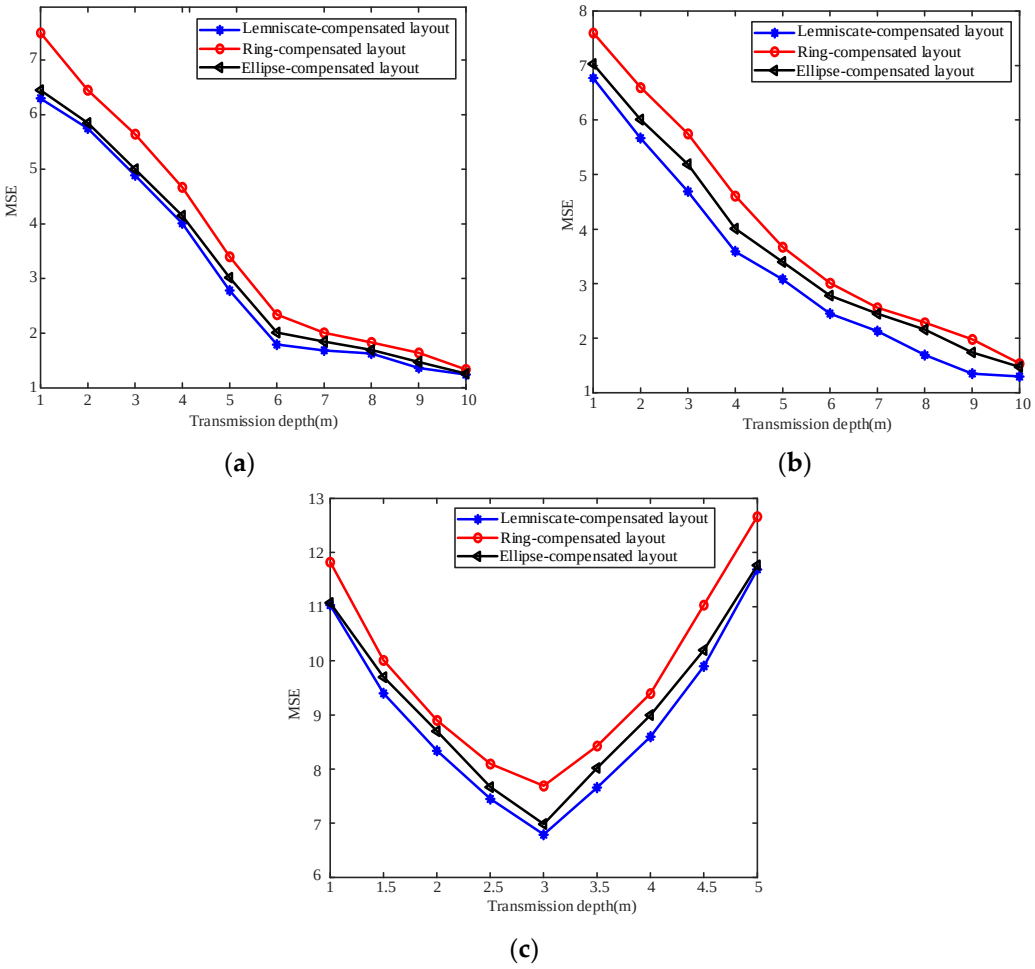

Figure 6. RMSE of the three LED layouts in (**a**) clean seawater; (**b**) coastal seawater; and (**c**) harbor seawater.

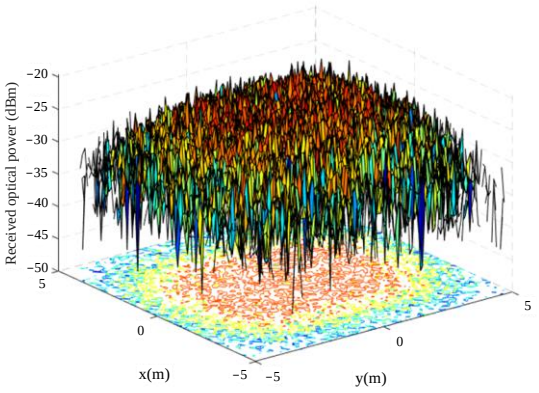

Figure 7. Received optical power distribution in harbor seawater at a depth of 5 m.

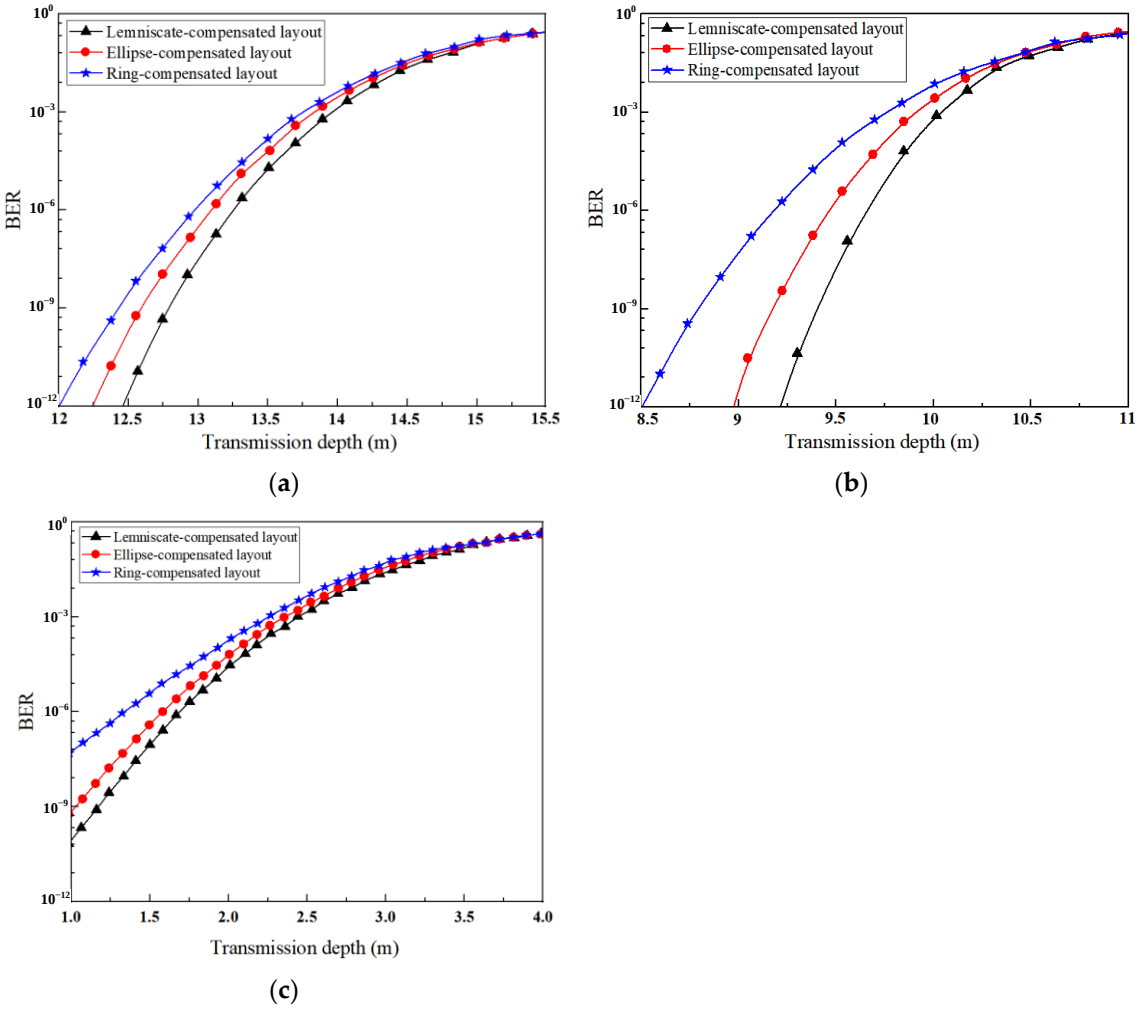

Figure 8. The BER performance of the three layouts in (**a**) clean seawater, (**b**) coastal seawater, and (**c**) harbor seawater.

4. Conclusions

In this paper, a lemniscate-compensated layout is proposed to enhance the coverage efficiency of the underwater LED array in the UOWC system. Based on the MC simulation method, the received optical power distribution and BER performance of the proposed system are analyzed under three typical seawater environments. At 5 m, 7 m, and 9 m transmission depths, the PPD values of the lemniscate-compensated LED layout are 0.79, 0.66, and 0.65, respectively, which can achieve a more stable power distribution of the received optical power. Through the analysis of RMSE results, the proposed LED layout shows better uniformity under three typical seawater environments. Furthermore, in clean and coastal seawater, the BER of the proposed LED layout demonstrates obvious advantages at the same transmission depth. In turbid harbor seawater, with the deterioration of seawater quality, the transmission distance of the system is limited. However, the proposed LED layout still achieves better BER performance. Furthermore, to verify the proposed LED array coverage model, an experimental verification system can be established in a real seawater environment to improve the underwater coverage performance of the LED array, which is of great significance to ensure the high-speed interconnection of underwater Internet of Things devices at short and medium ranges.

Author Contributions: Conceptualization, A.L. and H.Y.; formal analysis, A.L., H.Y. and H.Z.; methodology, A.L.; software, A.L., H.Y. and Y.Y.; validation, A.L. and Y.W.; writing—original draft, A.L., H.Y. and H.Z.; writing—review and editing, A.L. and Y.W.; visualization, A.L. and H.Y.; supervision, A.L.; project administration, A.L. and Y.W.; funding acquisition, A.L. and Y.W. All authors have read and agreed to the published version of the manuscript.

Funding: This work is supported in part by the Fundamental Research Funds for the Central Universities under Grant 3132023240, and the National Natural Science Foundation of China under Grants 62176037 and 62205045.

Data Availability Statement: The data presented in this paper are available after contacting the corresponding author.

Acknowledgments: The authors would like to thank the anonymous reviewers for their careful reading and valuable comments.

Conflicts of Interest: The authors declare no conflict of interest.

References

1. Song, G.; Xu, J. Review on Long-distance Underwater wireless optical communication. In Proceedings of the 2021 19th International Conference on Optical Communications and Networks (ICOCN), Qufu, China, 23–27 August 2021; pp. 1–4.
2. Liu, T.; Zhang, H.; Zhang, Y.; Song, J. Experimental demonstration of LED based underwater wireless optical communication. In Proceedings of the 2017 4th International Conference on Information Science and Control Engineering (ICISCE), Changsha, China, 21–23 July 2017; pp. 1501–1504.
3. Li, J.; Yang, B.; Ye, D.; Wang, L.; Fu, K.; Piao, J.; Wang, Y. A real-time, full-duplex system for underwater wireless optical communication: Hardware structure and optical link model. *IEEE Access* **2020**, *8*, 109372–109387. [CrossRef]
4. Li, J.; Wang, F.; Zhao, M.; Jiang, F.; Chi, N. Large-coverage underwater visible light communication system based on blue LED employing equal gain combining with integrated PIN array reception. *Appl. Opt.* **2019**, *58*, 383–388. [CrossRef] [PubMed]
5. Sahu, S.K.; Shanmugam, P. A theoretical study on the impact of particle scattering on the channel characteristics of underwater optical communication system. *Opt. Commun.* **2018**, *408*, 3–14. [CrossRef]
6. Gładysz, S.; Segel, M.; Montoya, J.; Toselli, I.; Gasperin, O.J.G.; Stein, K. Modelling, measurement and correction of underwater turbulence effects on optical communications. In Proceedings of the 2021 5th Underwater Communications and Networking Conference (UComms), Lerici, Italy, 31 August–2 September 2021; pp. 1–4.
7. Zhang, S.; Zhang, L.; Wang, Z.; Quan, J.; Cheng, J.; Dong, Y. On Performance of Underwater Wireless Optical Communications under Turbulence. In Proceedings of the 2020 IEEE 17th Annual Consumer Communications & Networking Conference (CCNC), Las Vegas, NV, USA, 10–13 January 2020.
8. Semernik, I.V.; Demyanenko, A.V.l.; Samonova, C.V.; Bender, O.V.; Tarasenko, A.A. Modelling of an underwater wireless optical communication channel. In Proceedings of the 2023 Radiation and Scattering of Electromagnetic Waves (RSEMW), Divnomorskoe, Russian, 26–30 June 2023; pp. 468–471.
9. Illi, E.; Bouanani, F.E.; Park, K.H.; Ayoub, F.; Alouini, M.S. An improved accurate solver for the time-dependent RTE in underwater optical wireless communications. *IEEE Access* **2019**, *7*, 96478–96494. [CrossRef]
10. Ma, T.; Du, Z.; Xu, J. Modeling for underwater optical channel in relatively turbid waters based on the Monte Carlo method. In Proceedings of the 2021 13th International Conference on Advanced Infocomm Technology (ICAIT), Yanji, China, 15–18 October 2021; pp. 122–127.
11. Geldard, C.T.; Thompson, J.; Leitgeb, E.; Popoola, W.O. Optical wireless underwater channel modelling in the presence of turbulence. In Proceedings of the 2018 IEEE British and Irish Conference on Optics and Photonics (BICOP), London, UK, 12–14 December 2018; pp. 1–4.
12. Yuan, R.; Ma, J.; Su, P.; Dong, Y.; Cheng, J. Monte-Carlo integration models for multiple scattering based optical wireless communication. *IEEE Trans. Commun.* **2019**, *68*, 334–348. [CrossRef]
13. Nezamalhosseini, S.A.; Chen, L.R. Optimal power allocation for MIMO underwater wireless optical communication systems using channel state information at the transmitter. *IEEE J. Ocean. Eng.* **2020**, *46*, 319–325. [CrossRef]
14. Ijeh, I.C.; Khalighi, M.A.; Elamassie, M.; Hranilovic, S.; Uysal, M. Outage probability analysis of a vertical underwater wireless optical link subject to oceanic turbulence and pointing errors. *J. Opt. Commun. Netw.* **2022**, *14*, 439–453. [CrossRef]
15. Liu, A.; Zhang, R.; Lin, B.; Yin, H. Multi-degree-of-freedom for underwater optical wireless communication with improved transmission performance. *J. Mar. Sci. Eng.* **2022**, *11*, 48. [CrossRef]
16. Ding, J.; Huang, Z.; Ji, Y. Evolutionary algorithm based power coverage optimization for visible light communications. *IEEE Commun. Lett.* **2012**, *16*, 439–441. [CrossRef]
17. Liu, H.; Lin, Z.; Xu, Y.; Chen, Y.; Pu, X. Coverage uniformity with improved genetic simulated annealing algorithm for indoor Visible Light Communications. *Opt. Commun.* **2019**, *439*, 156–163. [CrossRef]
18. Varma, G.P. Optimum power allocation for uniform illuminance in indoor visible light communication. *Opt. Express* **2018**, *26*, 8679–8689. [CrossRef] [PubMed]

19. Wang, J.; Xu, A.; Ju, J.; Guo, L. Optimization lighting layout of indoor visible light communication system based on improved artificial fish swarm algorithm. *J. Opt.* **2020**, *22*, 035701.
20. Huang, L.; Wang, P.; Wang, J.; Chi, S.; Niu, S.; Nan, X.; Che, H. Optimized design of the light source for an indoor visible light communication system based on an improved bat algorithm. *Appl. Opt.* **2020**, *59*, 10638–10644. [CrossRef]
21. Liu, A.; Yuan, Y.; Yin, H. Optimization of LED array spatial coverage characteristics in underwater wireless optical communication. *J. Mar. Sci. Eng.* **2023**, *11*, 253. [CrossRef]
22. Gabriel, C.; Khalighi, M.A.; Bourennane, S.; Léon, P.; Rigaud, V. Monte-Carlo-based channel characterization for underwater optical communication systems. *J. Opt. Commun. Netw.* **2013**, *5*, 1–12. [CrossRef]
23. Li, Y.; Qiu, H.; Chen, X.; Fu, J.; Musa, M.; Li, X. Spatial correlation analysis of imaging MIMO for underwater visible light communication. *Opt. Commun.* **2019**, *443*, 221–229. [CrossRef]
24. Zhang, J.; Kou, L.; Yang, Y.; He, F.; Duan, Z. Monte-Carlo-based optical wireless underwater channel modeling with oceanic turbulence. *Opt. Commun.* **2020**, *475*, 126214. [CrossRef]
25. Eso, E.; Ghassemlooy, Z.; Zvanovec, S.; Sathian, J.; Abadi, M.M.; Younus, O.I. Performance of Vehicular Visible Light Communications under the Effects of Atmospheric Turbulence with Aperture Averaging. *Sensors* **2021**, *21*, 2751. [CrossRef]
26. Jamali, M.V.; Salehi, J.A.; Akhoundi, F. Performance studies of underwater wireless optical communication systems with spatial diversity: MIMO scheme. *IEEE Trans. Commun.* **2016**, *65*, 1176–1192. [CrossRef]
27. Abshire, J.B. Performance of OOK and low-order PPM modulations in optical communications when using APD-based receivers. *IEEE Trans. Commun.* **1984**, *32*, 1140–1143. [CrossRef]
28. Che, H.; Wang, P.; Chi, S.; Sun, Y.; Yang, T.; Wang, Z. LED layout optimization in visible light communication system by a hybrid immune clonal bat algorithm. *Opt. Commun.* **2022**, *520*, 128532. [CrossRef]